Inorg. Chem. **2003**, *42*, 1590–1598

H-Bonding Dependent Structures of $(NH_4^+)_3H^+(SO_4^{2-})_2$. Mechanisms of Phase Transitions

Paulina M. Dominiak,[†] Joanna Herold,[‡] Waclaw Kolodziejski,[‡] and Krzysztof Woźniak*,[†]

Chemistry Department, Warsaw University, 02 093 ul. Pasteura 1, Warszawa, Poland, and Department of Inorganic and Analytical Chemistry, Medical University of Warsaw, ul. Banacha 1, 02-097 Warszawa, Poland

Received May 9, 2002

The role of different H-bonds in phases II, III, IV, and V of triammonium hydrogen disulfate, $(NH_4^+)_3H^+(SO_4^{2-})_2$, has been studied by X-ray diffraction and ^{1}H solid-state MAS NMR. The proper space group for phase II is *C*2/*c*, for phases III and IV is *P*2/*n*, and for phase V is $P\bar{1}$. The structures of phases III and IV seem to be the same. The hydrogen atom participating in the O^-–H^+···O^- H-bond in phase II of $(NH_4^+)_3H^+(SO_4^{2-})_2$ at room temperature is split at two positions around the center of the crucial O^-–H^+···O^- H-bonding, joining two SO_4^{2-} tetrahedra. With decreasing temperature, it becomes localized at one of the oxygen atoms. Further cooling causes additional differentiation of possibly equivalent sulfate dimers. The NH_4^+ ions participate mainly in bifurcated H-bonds with two oxygen atoms from sulfate anions. On cooling, the major contribution of the bifurcated H-bond becomes stronger, whereas the minor one becomes weaker. This is coupled with rotation of sulfate ions. In all the phases of $(NH_4^+)_3H^+(SO_4^{2-})_2$, some additional, weak but significant, reflections are observed. They are located between the layers of the reciprocal lattice, suggesting possible modulation of the host $(NH_4^+)_3H^+(SO_4^{2-})_2$ structure(s). According to ^{1}H MAS NMR obtained for phases II and III, the nature of the acidic proton disorder is dynamic, and localization of the proton takes place in a broader range of temperatures, as can be expected from the X-ray diffraction data.

Introduction

Triammonium hydrogen disulfate, $(NH_4^+)_3H^+(SO_4^{2-})_2$, is a member of a family of compounds which has the general formula $M_3H(XO_4)_2$, with M = NH_4^+, K^+, Na^+, Rb^+, Cs^+ and X = S, Se. The most characteristic feature of such compounds is a very strong O^-—H···O^- hydrogen bonding, joining two XO_4^{2-} ions, thus forming an isolated $H^+(XO_4^{2-})_2$ dimer (Figure 1). In the $(NH_4^+)_3H^+(SO_4^{2-})_2$ case, the situation is more complex because the NH_4^+ cations participate in numerous additional H-bonds.

Crystals of triammonium hydrogen disulfate undergo a series of phase transitions at 413, 265, 141, 133, and 63 K, forming six different phases.[1] The respective phases are denoted as I, II, III, IV, V, and VII with decreasing temperature. Under higher hydrostatic pressure, there is an additional phase denoted by VI.[2] Phase I is a superprotonic conductor, phase II is ferroelastic, phase III is antiferroelectric, and phase IV is incommensurate.[3] $(NH_4^+)_3H^+(SO_4^{2-})_2$

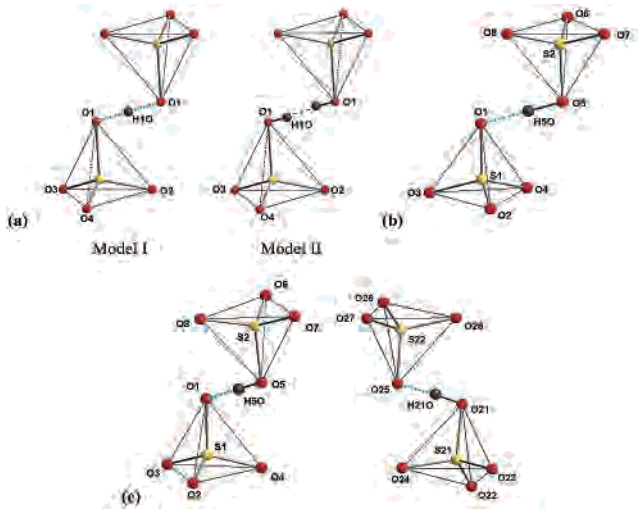

Figure 1. Projections of SO_4^{2-} tetrahedra: (a) in phase II (two models of possible H-bonding), (b) in phase III, (c) in phase V.

* Author to whom correspondence should be addressed. E-mail: kwozniak@chem.uw.edu.pl.
† Warsaw University.
‡ Medical University of Warsaw.

(1) Gesi, K. *Phys. Status Solidi A* **1976**, *33*, 479−482.

10.1021/ic025705b CCC: $25.00
Published on Web 01/30/2003

becomes ferroelectric under hydrostatic pressures higher than about 5 kbar in two phases (phases VI and VII).

The crystal structures of phases I and II are well known,[4−8] but for the other phases there are problems with finding their unique space groups.[5,8,9] In most phases, the differences between possible space groups depend on positions of hydrogen atoms participating in the H-bonds. This dependence of the space group on H-atom positions makes $(NH_4^+)_3H^+(SO_4^{2-})_2$ particularly interesting.

$(NH_4^+)_3H^+(SO_4^{2-})_2$ has attracted much attention so far. Among others, the deuterated form of letovicite was intensively studied.[10−15] The influence of isotope effect on ferroelectric activity—similar to the pressure consequences—is described in ref 16. Dielectric studies of phase transitions in $(NH_4^+)_3H^+(SO_4^{2-})_2$ within a broad range of temperatures were dealt with in refs 10, 17, 18, and 19. Connection between the ferroelastic properties of this compound and its structure is discussed in ref 20. The transformations between different phases of $(NH_4^+)_3H^+(SO_4^{2-})_2$ were characterized by calorimetric and dilatometric methods, electrical conductivity, and EPR spectroscopy.[21] The infrared and Raman spectra of $(NH_4^+)_3H^+(SO_4^{2-})_2$ are discussed in 22, 23, and 24. Possible space group assignment for a few phases is proposed[9] on the basis of oscillation photos. Even topographic properties of $(NH_4^+)_3H^+(SO_4^{2-})_2$ were studied using synchrotron radiation[21] and an optical polarizing microscope.[20,25] Powder diffraction studies of phase I of $(NH_4^+)_3H^+(SO_4^{2-})_2$ are discussed in ref 6. Different properties of new compounds obtained by substitution of the cations in $(NH_4^+)_3H^+(SO_4^{2-})_2$ by Rb^+ were examined in refs 26−29.

Because there are different structural results published so far for this compound,[3−9,14] we have decided to perform careful investigations of these phases to clear up the situation. So, in this work, we report the structures of phases II, III, IV, and V, collected with a CCD diffractometer. We think that the technological progress with X-ray detectors is, in this case, very important, because properties of all these phases depend on the weakest reflections, which, in fact, were missed quite often when old types of sequential detectors were used. As a consequence of more reliable data collection, a number of important new phenomena can be observed. For example, we found that in all the phases of $(NH_4^+)_3H^+(SO_4^{2-})_2$, there are weak interlayer reflections with fractional indexes, which may result from a modulation of such structures. Such a modulation was observed for one phase,[3] but it appears that with better tools it can be found for all of the phases.

The next important issue is the mechanisms of phase transitions which we would like to establish on the basis of X-ray and solid-state NMR data. To avoid symmetry constraints, we applied the ^1H MAS solid-state NMR technique. Such an alternative method gives complementary information about hydrogen bonding.

Experimental Section

X-ray Diffraction. Single crystals of $(NH_4^+)_3H^+(SO_4^{2-})_2$ were grown from water solution by the slow evaporation method.[28] All measurements of diffractional data were accomplished on a Kuma KM4CCD κ-axis diffractometer with graphite-monochromated Mo Kα radiation. A monocrystal was positioned at 60 mm from the KM4CCD camera. For all the measurements, 636 frames were collected with the ω-scan at 2.0° intervals with a counting time of 5 s. For variable temperature measurements, an Oxford Cryostream attachment was used. The data were corrected for Lorentz and polarization effects. No absorption correction was applied because of the small linear absorption coefficient (0.623 mm^{-1}); the data corrected and uncorrected for absorption gave the same results on refinement. Data reduction and analysis were carried out with the Kuma Diffraction (Wrocław, Poland) suite of programs.

The structures were solved by direct methods[30] and refined using SHELXTL.[31] The refinement was based on F^2 for all reflections. Weighted R factors wR and all goodness-of-fit *S* values are based on F^2. Conventional R factors are based on *F* with *F* set to zero for negative F^2. The $F_o^2 > 2\sigma(F_o^2)$ criterion was used only for calculating *R* factors and is not relevant to the choice of reflections for the refinement. The *R* factors based on F^2 are about twice as large as those based on *F*. All hydrogen atoms were located from

(2) Gesi, K.; Ozawa, K. *J. Phys. Soc. Jpn.* **1977**, *43*, 570−574.
(3) Fukami, T.; Horiuchi, K.; Nakasone, K.; Furukawa, K. *Jpn. J. Appl. Phys., Part 1* **1996**, *35* (4A), 2253−2254.
(4) Schwalowsky, L.; Adiwidjaja, G.; Friese, K.; Meyer, H.-W.; Röwer, R.-W. $(NH_4^+)_3H^+(SO_4^{2-})_2$, *Hasylab Annual Report* **1996**, 679−680.
(5) Sooryanarayana, K.; Row, G. T. N. *Phase Transitions* **1996**, *58* (4), 263−271.
(6) Suzuki, S.; Makita, Y. *Acta Crystallogr. B* **1978**, *34*, 732−735.
(7) Leclaire, A.; Ledesert, M.; Monier, J. C.; Daoud, A.; Damak, M. *Acta Crystallogr. B* **1985**, *41*, 209−213.
(8) Sooryanarayana, K.; Row, G. T. N.; Robinson, W. T. *Phase Transitions* **1999**, *69(4)*, 429−438.
(9) Chen, R. H.; Wang, L. M. Yang, S. C. *Phase Transitions* **1992**, *37*, 141−147.
(10) Osaka, T.; Makita, Y.; Gesi, K. *J. Phys. Soc. Jpn.* **1980**, *49*, 593−598.
(11) Tanaka, M.; Shiozaki, Y. *Acta Crystallogr. B* **1981**, *37*, 1171−1174.
(12) Tanaka, M.; Shiozaki, Y. *Acta Crystallogr. C* **1986**, *42*, 776−780.
(13) Fukami, T.; Ninomiya, H.; Chen, R. H. *Solid State Ionics* **1997**, *98* (1−2), 105−111.
(14) Tamura, I.; Noda, Y.; Morii, Y. *J. Phys. Chem. Solids* **1999**, *60* (8−9), 1411−1414.
(15) Fukami, T.; Horiuchi, K.; Chen, R. H. *Solid State Ionics* **2000**, *131* (3−4), 275−280.
(16) Ichikawa, M. *Pol. J. Chem.* **1998**, *72* (2), 230−240.
(17) Gesi, K. *Jpn. J. Appl. Phys.* **1980**, *19*, 1051−1053.
(18) Schwalowsky, L.; Vinnichenko, V.; Baranov, A.; Bismayer, U.; Merinov, B.; Eckold G. *J. Phys.*: *Condens. Matter*. **1998**, *10* (13), 3019−3027.
(19) Chen, R. H.; Chen, T. M.; Shern, C. S. *J. Phys. Chem. Solids* **2000**, *61* (9), 1399−1406.
(20) Schwalowsky, L.; Bismayer, U.; Lippmann, T. *Phase Transitions* **1996**, *59* (1−3), 61−76.
(21) Becker, R. A.; Docherty, R.; El-Korashy, A.; Jennissen, H.-D.; Klapper, H.; Roberts, K. J. *Phase Transitions* **1992**, *39*, 171−183, and the references therein.
(22) Damak, M.; Kamoun, M.; Daoud, A.; Romain, F.; Lautie, A.; Novak, A. *J. Mol. Struct.* **1985**, *130*, 245−254.
(23) Videnova-Adrabinska, V. *J. Mol. Struct.* **1991**, *244*, 203−222.
(24) Besbes, H.; Mhiri, T.; Daoud A. *Phase Transitions* **1999**, *70* (3), 183−195.
(25) Chen, R. H.; Chen, T. M. *J. Phys. Chem. Solids* **1997**, *58* (1), 161−&.
(26) Bronowska, W.; Videnova-Adrabinska, V.; Pietraszko, A. *Ferroelectrics* **1995**, *172*, 411−417.
(27) Bronowska, W.; Pietraszko, A. *J. Mol. Struct.* **1996**, *374*, 171−175.
(28) Baranov, A. I.; Dolbinina, V. V.; Yakushkin, E. D.; Vinnichenko, V. Yu.; Lanceros-Mendez, S. *Ferroelectrics* **1998**, *217*, 285−295.
(29) Smirnov, L. S.; Baranov, A. I.; Shuvalov, L. A.; Bobrowicz-Sarga, L.; Natkaniec, I.; Waplak, S. *Phys. Solid State* **2001**, *43* (1), 117−126.
(30) Sheldrick, G. M. *Acta Crystallogr. A* **1990**, *46*, 467−473.
(31) Sheldrick G. M. *SHELXTL97. Program for the Refinement of Crystal Structures*; University of Göttingen, Germany.

Table 1. Crystallographic Data for Different Phases of $(NH_4^+)_3H^+(SO_4^{2-})_2$[a]

phase	II	III	IV	V
chem form	$N_3H_{13}S_2O_8$	$N_3H_{13}S_2O_8$	$N_3H_{13}S_2O_8$	$N_3H_{13}S_2O_8$
fw	247.25	247.25	247.25	247.25
temp [K]	rt	150(1)	136(1)	120(1)
λ [Å]	0.71073	0.71073	0.71073	0.71073
space group	*C*2/*c*	*P*2/*n*	*P*2/*n*	$P\bar{1}$
a [Å]	15.390(3)	10.044(2)	10.048(2)	8.267(2) [15.534][b]
b [Å]	5.848(1)	5.813(1)	5.806(1)	10.081(2) [5.792][b]
c [Å]	10.140(2)	15.540(3)	15.538(3)	11.585(2) [10.081][b]
α [deg]	90	90	90	90.46(3) [90.46][b]
β [deg]	101.81(3)	101.58(3)	101.55(3)	110.04(3) [101.48][b]
γ [deg]	90	90	90	100.62(3) [89.53][b]
vol [Å^3]	893.3(3)	888.8(3)	888.1(3)	888.8(3) [888.8(3)][b]
Z	4	4	4	4
ρ_{calc} [Mg/m^3]	1.838	1.848	1.849	1.848
μ(Mo Kα) [mm^{-1}]	0.623	0.626	0.626	0.626
R1 [c] (I > 2)	0.0369	0.0347	0.0399	0.0405
wR2 [d] (I > 2)	0.0900	0.0935	0.1113	0.1196
R1 [c] (all)	0.0434	0.0426	0.0510	0.0512
wR2 [cd] (all)	0.0957	0.0997	0.1209	0.1269
θ range [deg]	3.74−28.80	3.50−28.78	3.51−28.77	3.13−28.77
refl collect	7795	15419	15480	16194
data / param.	1115/86	2220/172	2228/172	4332/340
largest diff. peak and hole	0.484, −0.514	0.377, −0.601	0.407, −0.706	0.532, −0.718

[a] Literature data for different phases. Phase I: $R\bar{3}m$,[4,5] $T = 413$ K:[5] $a = 5.906(1)$ Å, $b = 5.906(1)$ Å, $c = 22.602(1)$ Å, α, $\beta = 90°$, $\gamma = 120°$, V = 682.8 Å^3, $R_{all} = 0.104$, or $R\bar{3}$[4] $T = 430$ K: $a = 5.907(2)$ Å, $b = 5.907(2)$ Å, $c = 22.549(7)$ Å, α, $\beta = 90°$, $\gamma = 120°$, $V = 681.4$ Å^3, $R_{all} = 0.0486$. Phase II: *A*2/*a*,[6] room temperature, $a = 10.153(3)$ Å, $b = 5.854(2)$ Å, $c = 15.410(6)$ Å, $\beta = 101.76(2)°$, $V = 896.7$ Å^3, $R_{all} = 0.045$ or *C*2/*c*[7] with $a = 15.435(2)$ Å, $b = 5.865(1)$ Å, $c = 10.1696(8)$ Å, $\beta = 101.829(8)°$, $V = 901.1$ Å^3, $R_{all} = 0.029$ or *C*2.[9] Phase III: *C*2/*c*[5] $T = 163$ K, $a = 15.578(4)$ Å, $b = 5.816(1)$ Å, $c = 10.050(4)$ Å, $\beta = 101.58(3)°$, $V = 892.0$ Å^3, $R_{all} = 0.031$ or *P*2/*n*[8] or *Pn*.[10] Phase V: *C*2.[8] [b] Conventional choice of the monoclinic *C* cell; [c] $R1 = \sum||F_o| - |F_c||/\sum|F_o|$. [d] $wR2 = [\sum[w(F_o^2 - F_c^2)^2]/\sum[w(F_o^2)^2]]^{1/2}$.

difference maps and refined isotropically. Scattering factors were taken from Tables 6.1.1.4 and 4.2.4.2 in ref 32.

Solid-State NMR. Variable-temperature solid-state ^{1}H NMR spectra were measured with a Bruker AVANCE 400 WB spectrometer at 400.1 kHz. The spectra were recorded under magic-angle spinning (MAS) at 12 kHz, using a $\pi/2$ pulse of 2.6 μs and a recycle delay of 6 s. The 4 mm ZrO_2 rotor was spun with dry air, and the temperature inside the rotor was calibrated with the ^{207}Pb thermometer.[33] The peaks were deconvoluted and fitted on a PC computer using the NUTS program.[34]

Results and Discussion

Space Group Symmetry. We collected the X-ray data for four phases: phase II at room temperature, phase III at 150 K, phase IV at 136 K, and phase V at 120 K. All the measurements were accomplished on the same monocrystal. Structural data obtained for all these phases are summarized in Table 1 which also contains proper reference literature data. Geometry of SO_4^{2-} tetrahedra in all phases is given in Table 2.

According to our results, phase II has *C*2/*c* space group symmetry with unit cell parameters $a = 15.390(3)$ Å, $b = 5.848(1)$ Å, $c = 10.140(2)$ Å, and $\beta = 101.81(3)°$. The proper space group for phase III at 150 K is *P*2/*n* with unit cell parameters $a = 10.044(2)$ Å, $b = 5.813(1)$ Å, $c = 15.540(3)$ Å, $\beta = 101.58(3)°$ and for phase IV at 136 K is *P*2/*n* with $a = 10.048(2)$ Å, $b = 5.806(1)$ Å, $c = 15.538(3)$ Å, and $\beta = 101.55(3)°$. The structure of phase IV seems to be very similar to that of phase III if not the same. Chen et al.[9] reported that they also did not detect this phase transition from X-ray precision pictures. Phase V has $P\bar{1}$ space group symmetry with unit cell parameters $a = 8.267(2)$ Å, $b = 10.081(2)$ Å, $c = 11.585(2)$ Å, $\alpha = 90.46(3)°$, $\beta = 110.04(3)°$, and $\gamma = 100.62(3)°$. Unfortunately, it appeares that the highest temperature phase is quite difficult to achieve because there is a significant powdering of monocrystals at temperatures above 400 K.

The Main Structure. Our investigations indicate that there is a quite significant degree of similarity among the structures of all these phases, i.e., II, III, IV, and V. According to X-ray results in each phase, there are 8 sulfate and 12 ammonium ions in the unit cell. The unit cell contents for all the phases are shown in Figure 2, with the independent parts of the unit cell in the foreground and the rest of the moieties marked in the background.

There are two sets of the ammonium ions which have different topology from that of their closest neighborhood. The first class of ammonium ions is in a general position; whereas, in the case of the second class, the NH_4^+ ions are in a special position at 2-fold axis. In the case of the lowest symmetry phase V, all the ammonium ions are in general positions, although there are still two types.

Two neighboring sulfate ions form an isolated dimer via a strong ionic $O^--H^+\cdots O^-$ hydrogen bond. The other oxygen atoms of the SO_4^{2-} polyhedron participate in a network of $N^+-H\cdots O^-$ hydrogen bonds, which is well illustrated in Figure 3. These H-bonds form a starlike motif. The repetition of such motives in the crystal lattice gives chains of hydrogen bonds which were first reported by Leclaire et al.[7] These chains altogether build a 2D platform

(32) *International Tables for X-ray Crystallography*; Macgillavry, C. H., Rieck G. D., Eds.; Kynoch Press: Birmingham, England, 1962; Vol. III..
(33) Bielecki, A.; Burum, D. P. *J. Magn. Reson.* **1995**, *A116*, 215−220.
(34) *NUTS NMR Data Processing Software Version 4.96*; Acorn NMR Inc., Fremont, U.S.A.

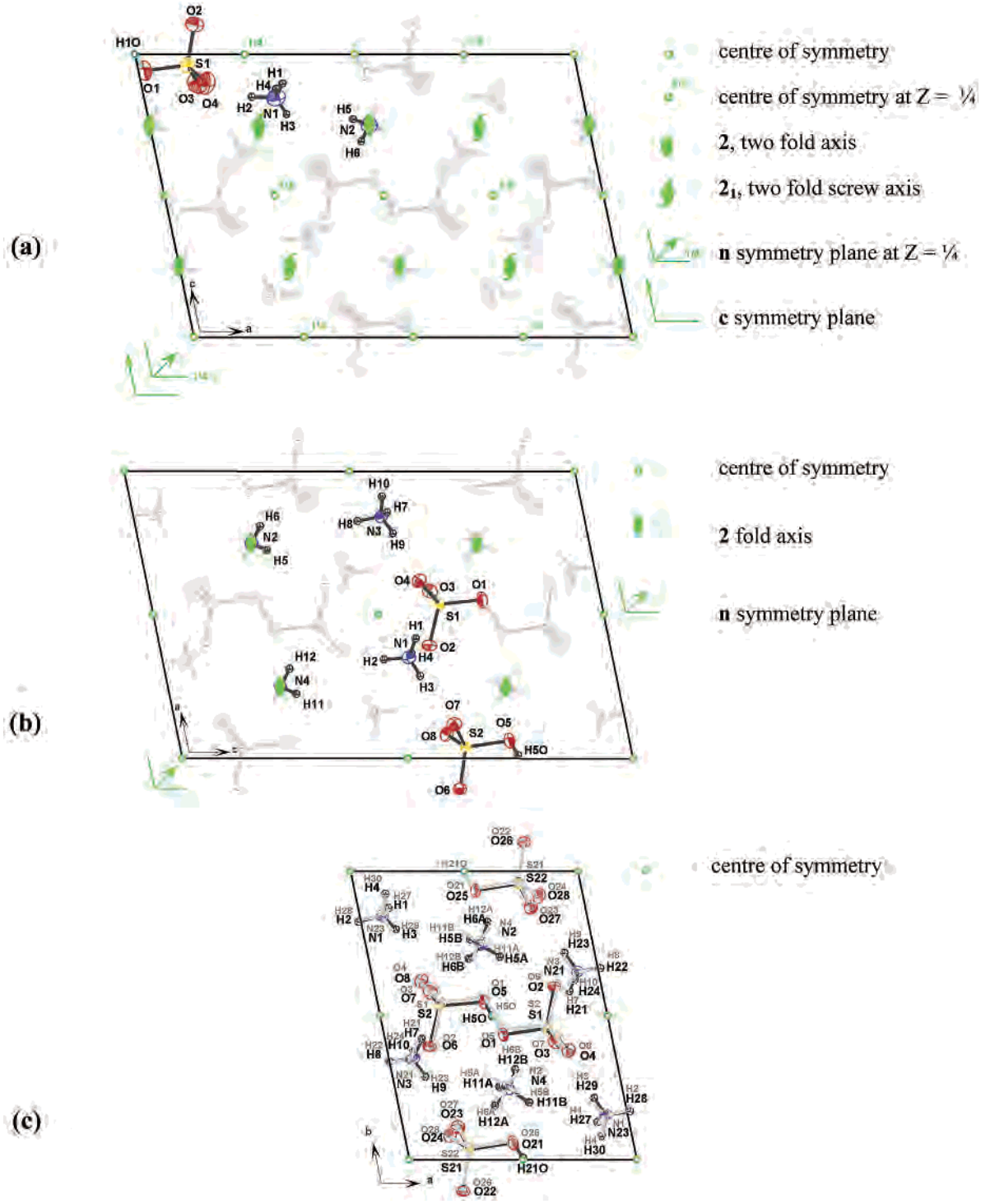

Figure 2. Symmetry elements, numbering schemes, and atomic displacement parameters for $(NH_4^+)_3H^+(SO_4^{2-})_2$: (a) in phase II, space group *C*2/*c*; (b) in phase III, space group *P*2/*n*; (c) in phase V, space group $P\bar{1}$. An independent part of the unit cell is shown in the foreground, and symmetry related molecules are shown in the background. Symmetry elements are defined on the right-hand side. Thermal ellipsoids are drawn at the 50% probability level.

based on oxygen atoms which are not involved in the $O^-{-}H^+{\cdots}O^-$ H-bond. Such planes are arranged head-to-head in parallel stacks. These planes are linked together by NH_4^+ ions via $N^+{-}H{\cdots}O^-$ and $O^-{-}H^+{\cdots}O^-$ H-bonds on the one side and by $N^+{-}H{\cdots}O^-$ H-bonds on the other side. Both these ammonium ions belong to different classes.

Mechanism of Phase Transitions. Cooling down of $(NH_4^+)_3H^+(SO_4^{2-})_2$ monocrystals is accompanied by gradual ordering of molecules in the crystal lattice and, in consequence, decrease of symmetry. In phase II, the independent part of the unit cell consists of one sulfate ion and one and a half ammonium ions (see Figure 2). In phases III and IV, there are two independent sulfate and three ammonium ions. Also, in phase V, four sulfate and six ammonium ions form the independent part of the unit cell.

Figure 4 illustrates how particular atoms change their positions during the phase transitions. These plots were made by finding the best fit of atomic positions in one phase to

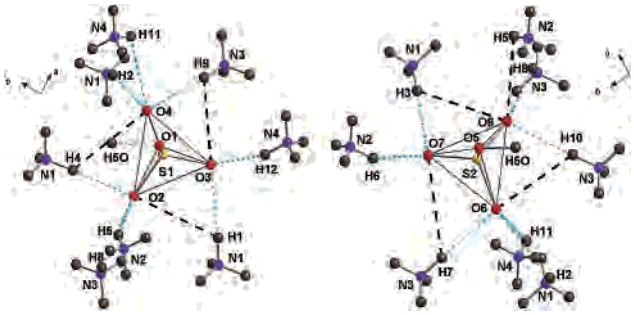

Figure 3. H-bond network around SO_4^{2-} and NH_4^+ polyhedra in phase III at 150 K. The weakest H-bonds are marked by dashed lines.

Table 2. Bond Lengths [Å] and Bond Angles [deg] Calculated for SO_4^{2-} Tetrahedra in Different Phases

phase II		
	model I	model II
S(1)−O(4)	1.446(2)	1.445(2)
S(1)−O(3)	1.448(2)	1.448(2)
S(1)−O(2)	1.452(2)	1.452(2)
S(1)−O(1)	1.519(2)	1.518(2)
O(4)−S(1)−O(3)	111.6(1)	111.7(1)
O(4)−S(1)−O(2)	111.2(1)	111.2(1)
O(3)−S(1)−O(2)	111.3(1)	111.3(1)
O(4)−S(1)−O(1)	107.5(1)	107.6(1)
O(3)−S(1)−O(1)	107.6(1)	107.5(1)
O(2)−S(1)−O(1)	107.3(1)	107.4(1)

phase III			
S(1)−O(4)	1.461(1)	S(2)−O(8)	1.457(1)
S(1)−O(3)	1.460(1)	S(2)−O(7)	1.456(1)
S(1)−O(2)	1.467(1)	S(2)−O(6)	1.458(1)
S(1)−O(1)	1.506(1)	S(2)−O(5)	1.534(1)
O(4)−S(1)−O(3)	111.20(7)	O(8)−S(2)−O(7)	112.41(7)
O(4)−S(1)−O(2)	110.96(7)	O(8)−S(2)−O(6)	111.38(7)
O(3)−S(1)−O(2)	110.70(7)	O(7)−S(2)−O(6)	111.82(7)
O(4)−S(1)−O(1)	108.06(7)	O(8)−S(2)−O(5)	107.23(7)
O(3)−S(1)−O(1)	108.15(7)	O(7)−S(2)−O(5)	106.38(7)
O(2)−S(1)−O(1)	107.63(8)	O(6)−S(2)−O(5)	107.23(8)

phase V			
S(1)−O(4)	1.460(2)	S(2)−O(8)	1.452(2)
S(1)−O(3)	1.464(2)	S(2)−O(7)	1.454(2)
S(1)−O(2)	1.473(2)	S(2)−O(6)	1.460(2)
S(1)−O(1)	1.502(2)	S(2)−O(5)	1.536(2)
O(4)−S(1)−O(3)	111.0(1)	O(8)−S(2)−O(7)	112.3(1)
O(4)−S(1)−O(2)	110.6(1)	O(8)−S(2)−O(6)	112.0(1)
O(3)−S(1)−O(2)	110.5(1)	O(7)−S(2)−O(6)	111.9(1)
O(4)−S(1)−O(1)	108.3(1)	O(8)−S(2)−O(5)	107.0(1)
O(3)−S(1)−O(1)	108.7(1)	O(7)−S(2)−O(5)	106.2(1)
O(2)−S(1)−O(1)	107.6(1)	O(6)−S(2)−O(5)	106.9(1)
S(21)−O(24)	1.457(2)	S(22)−O(28)	1.469(2)
S(21)−O(23)	1.449(2)	S(22)−O(27)	1.465(2)
S(21)−O(22)	1.458(2)	S(22)−O(26)	1.473(2)
S(21)−O(21)	1.549(2)	S(22)−O(25)	1.496(2)
O(24)−S(1)−O(23)	112.5(1)	O(28)−S(2)−O(27)	110.7(1)
O(24)−S(1)−O(22)	112.3(1)	O(28)−S(2)−O(26)	110.3(1)
O(23)−S(1)−O(22)	112.2(1)	O(27)−S(2)−O(26)	110.4(1)
O(24)−S(1)−O(21)	106.8(1)	O(28)−S(2)−O(25)	108.3(1)
O(23)−S(1)−O(21)	105. 7(1)	O(27)−S(2)−O(25)	109.4(1)
O(22)−S(1)−O(21)	106.8(1)	O(26)−S(2)−O(25)	108.0(1)

the model built of atomic positions in the neighboring phase. During the phase transition II/III, only one of the two types of ammonium tetrahedra—the N(1) tetrahedron—rotates by a few degree (ca. 13° and ca. 31°). This rotation is accompanied by rotation of the sulfate tetrahedron in the O(2)O(3)O(4) plane (ca. 8°). The ammonium N(2) tetrahedron does not significantly change its position. No difference was observed between phases III and IV. Through the phase transition IV/V only one sulfate tetrahedron rotates (ca. 14°) of the two independent tetrahedra forming the dimer. Also both types of the nitrogen tetrahedra rotate and shift slightly their positions in the crystal lattice.

O^-−H^+···O^- Hydrogen Bonding. The crucial point related to the above phase transitions of $(NH_4^+)_3H^+(SO_4^{2-})_2$ is the position of the hydrogen atom in the O^-···H^+···O^- H-bonding. Geometry of all such bonds in all phases is given in Table 3. In phase II, a proper model of H-bonding has to be chosen. The atom H(1O) participating in this H-bond could either be in a special position at the center of symmetry (model I) or be split in two positions around this center (model II; see Figure 1). The other atoms are refined in the same positions in both models. Difference Fourier maps around H(1O)—calculated when this H-atom is excluded from calculations—indicate that model II is closer to reality, Figure 5.

In phases III and IV the hydrogen atom is evidently more bonded to the O(5) oxygen atom than to O(1). This situation breaks the symmetry between the sulfate ions and, in consequence, generates nonidentical changes in the S(1)-O(1) and S(2)O(5) bond lengths. So, these changes in the O(5)−H(5O)···O(1) hydrogen bond are the main reason of the phase transition from space group *C*2/*c* to P2/n (from phase II to phase III). As we already mentioned we do not see any differences between phases III and IV. Whereas, in phase V, the crucial hydrogen atoms are also localized at oxygens and additionally there are two different sulfate dimers with different hydrogen bonds: O(1)···H(5O)−O(5) and O(21)−H(21O)···O(5). These two pairs of dimers form along the Z-axis two different columns of $H^+(SO_4^{2-})_2$ anions. Contrary to phases III and IV, two neighboring $H^+(SO_4^{2-})_2$ dimers have their H-atoms at the opposite sides of the column axis (for phase V see Figure 2).

N^+−H···O^- Hydrogen Bonding. Most of the N^+−H··· O^- H-bonds are bifurcated (one donor N−H group and two accepting oxygen atoms). In most cases both accepting oxygens come from the same sulfate moiety; however for some H-bonds both oxygens come from two different sulfate ions. When one applies a limit for the donor···acceptor distance (we use 3.3 Å), one obtains only a few nonbifurcated H-bonds, for example, in phase II, N(2)H(6)···O(3) [$-X + {}^1/_2$, $Y - {}^1/_2$, $-Z + {}^3/_2$]; in phase III, N(2)H(6)···O(7) [$-X + 1$, $-Y + 1$, $-Z + 1$] and N(4)H(12)···O(3)[$-X + 1$, $-Y$, $-Z + 1$] and in phase V, N(2)H(6A)···O(23) [$-X + 1$, $-Y + 1$, $-Z + 1$], N(2)H(6B)···O(3) [$-X + 1$, $-Y + 1$, $-Z + 1$], N(4)H(12A)···O(27) [$-X + 1$, $-Y + 1$, $-Z$] and N(4)-H(12B)···O(7) [$-X + 1$, $-Y + 1$, $-Z$]. The bifurcated H-bonds are weaker than the nonbifurcated ones. Geometries of all N^+−H···O^- H-bonds are given in the Supporting Information (see Table S1).

With decreasing temperature the weaker H-bonds participating in the N^+−H···2O^- H-bonding become even weaker, whereas the stronger ones become even stronger (Figures 6 and 3). Additionally, from Figure 3 one can see that the distribution of weak and strong H-bonds indicates a relative rotation of both the sulfate and ammonium ions resulting from changes in the strength of the H-bonds. This phenom-

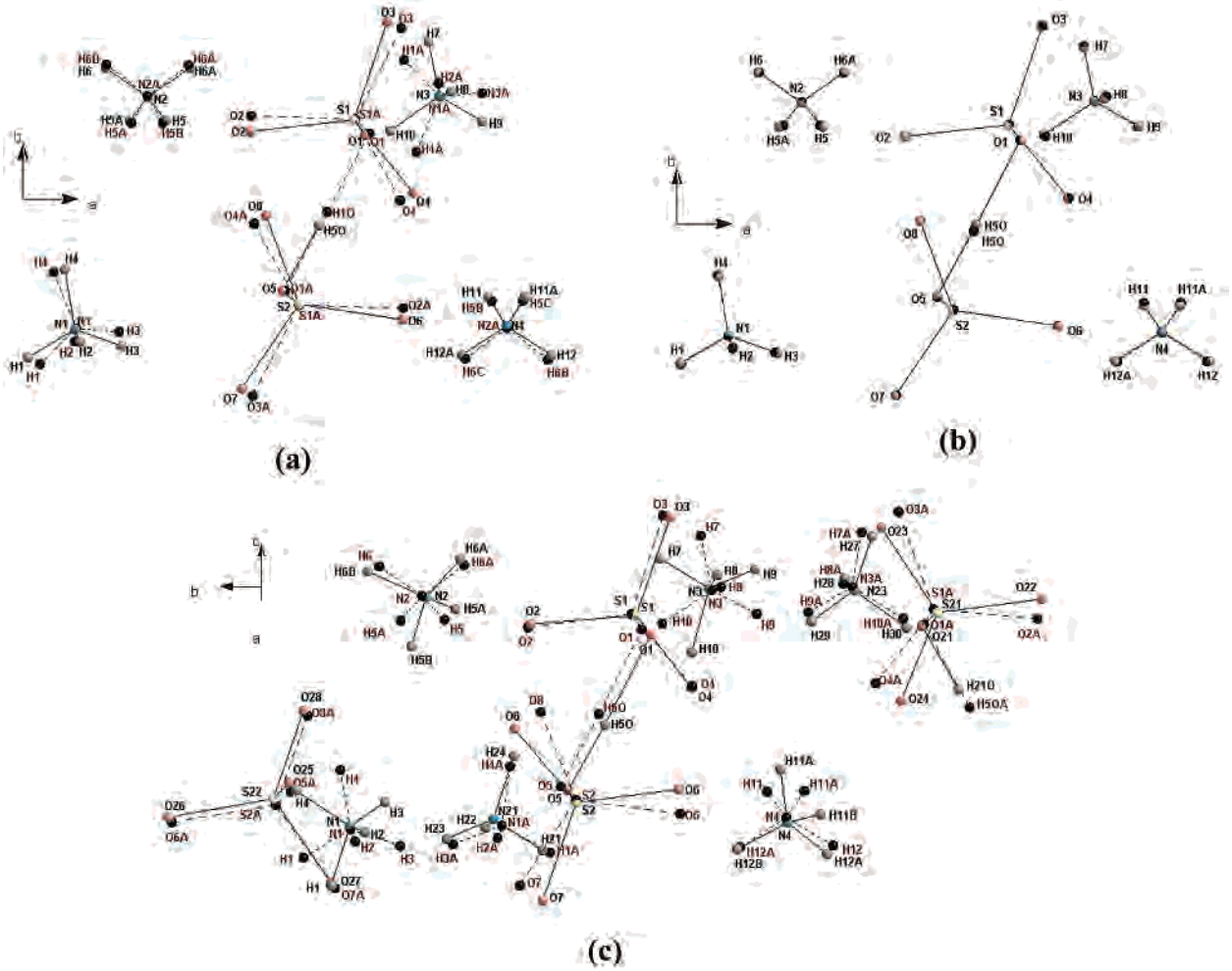

Figure 4. Illustration of phase transitions: (a) phases II/III, (b) phases III/IV, (c) phases IV/V. Dotted lines denote phases II, III, and IV, and solid lines denote phases III, IV, and V on plots a, b, and c, respectively.

Table 3. $O^-\cdots H^+\cdots O^-$ H-Bond Geometry in Different Phases of $(NH_4^+)_3H^+(SO_4^{2-})_2$

phase donor−H···acceptor	accepting atom symmetry code	D−H [Å]	H···A [Å]	D···A [Å]	D−H···A [deg]
phase II					
O(1)···H(1O)···O(1) model I	$-X, -Y, 2-Z$	1.270(2)	1.270(2)	2.540(6)	180.0(1)
O(1)−H(1O) H(1O)−O(1) model II	$-X, -Y, 2-Z$	0.70(5)	1.85(4)	2.550(6)	176.3(1)
phase III					
O(5)−H(5O)···O(1)	$0.5-X, Y, 1.5-Z$	1.07(4)	1.45 (3)	2.521(6)	178.2(1)
phase V					
O(5)−H(5O)···O(1)		1.07(4)	1.44(4)	2.513(3)	177.6(2)
O(21)−H(21O)···O(25)	$X, -1+Y, Z$	1.06(5)	1.47(2)	2.534(3)	176.4(2)

enon maybe quantified in a number of relations among H-bond structural parameters. Figure 6 presents such a characteristic relation between N···O and H···O distances. Starting from medium strength H-bonds in phase II, one gets both stronger and weaker H-bonds in phases III (IV) and V. This is independent of the ammonium nitrogen type.

Consequences of Interlayered Reflections. One of the great advantages of CCD diffractometers is this that one collects all the reflections present in defined regions of the reciprocal lattice. This is not the case for the sequential detectors because they require known parameters of the unit cell (which are established on the basis of strong reflections randomly found in the reciprocal lattice). Then only those reflections which fulfill Bragg's law are collected. This may lead to the situation that weak reflections are missed when old type diffractometers are used. During our studies of $(NH_4^+)_3H^+(SO_4^{2-})_2$, we observed some weak interlayered reflections beside the host reflections. These reflections are about 3 orders of magnitude less intense, but they still are significant. This situation was carefully tested to avoid the $\lambda/2$ contamination effect,[35] so this is not the case; even with proper lowering of voltage down to ca. 35 kV, these weak reflections were still found. Such reflections are best visible for phase IV; however when the data collection time is long enough they can be observed for the other phases too. Figure 7 presents one of the reciprocal lattice layers for phase IV.

(35) Kirschbaum, K.; Martin, A.; Pinkerton, A. A. *J. Appl. Crystallogr.* **1997**, *30*, 514−516.

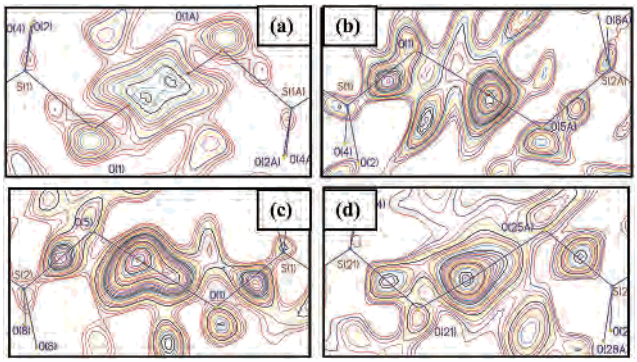

Figure 5. (F_o-F_c) difference electron density maps: (a) phase II in the region of H(1O) in the S(1)O(1)S(1A)O(1A) plane (label A stands for atoms related by a symmetry center); (b) phase III in the region of H(5O) in the S(2)O(1)S(2A)O(5A) plane (label A denotes second independent moiety); (c) phase V in the region of H(5O) in the S(1)O(1)S(2)O(5) plane; (d) phase V, in the region of the H(21O) atom in the S(21)O(21)S(22A)O(25A) plane (label A denotes the second independent moiety in the closest neighborhood). Contours are plotted, starting from 0.0 e/Å^3, every 0.025 e/Å^3. Black dots denote crucial H-atom positions.

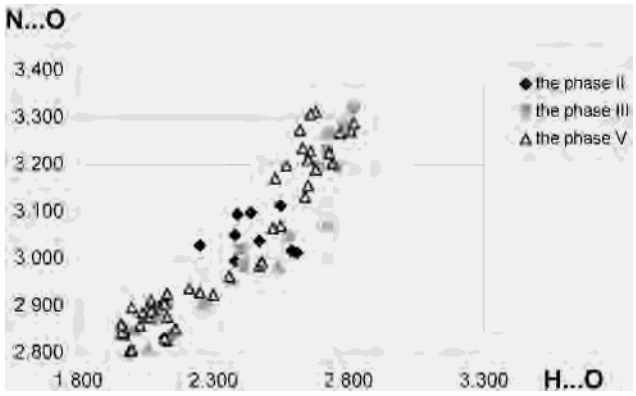

Figure 6. Relationships between N···O and H···O distances in $N^+-H\cdots O^-$ H-bonding.

The interlayered reflections should have partial indexes. Taking them into account does not allow refinement of the structures either in the known space groups or in new ones. Such a situation suggests possible modulation of these structures. The presence of a modulation, particularly in phase IV, creates additional problems in rationalization of the phase transitions and changes of electric properties of these crystals as a function of temperature. In this work, we describe just the first approximated model of structures of different phases. These are so-called host structures. However, to achieve full description of these phase transitions, additional investigations (neutrons, modulated structure refinement) are required. They are ongoing projects in our lab.

We also want to pinpoint that in the case of $(NH_4^+)_3H^+(SO_4^{2-})_2$ location of the proton is strongly dependent on diffraction angle, which influences not only the values of structural parameters (bond lengths and angles) but also the assignment of the space group symmetry for a given phase. This is probably one of the reasons why such different structural data for this compound can be found in the literature.

Solid-State NMR. The proton MAS spectra were recorded in the 235−381 K temperature range. Within this range, two

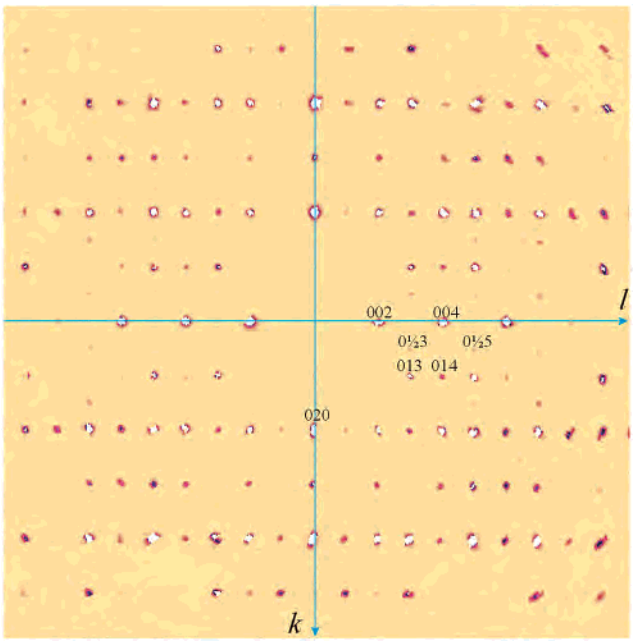

Figure 7. (0*kl*) reciprocal lattice layer (conventional choice of the monoclinic *C* cell) for phase IV at 136 K.

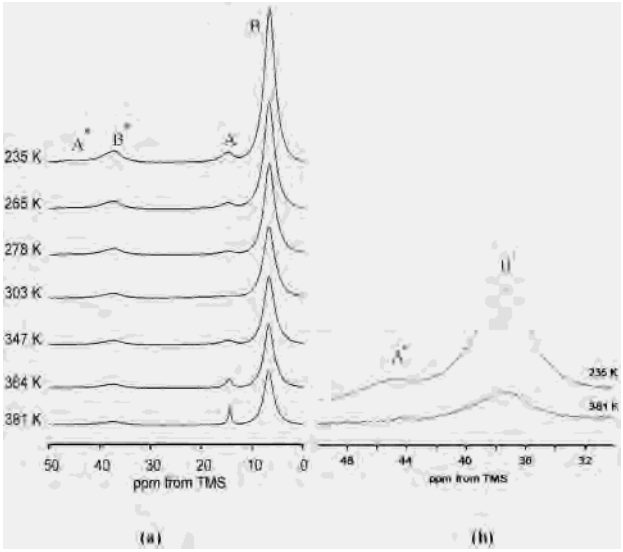

Figure 8. Selected ^{1}H MAS NMR spectra of letovicite: (a) variable-temperature spectra, (b) first high-frequency rotational sidebands. Letters A and B denote peaks from the acidic protons of the $O^-\cdots H^+\cdots O^-$ hydrogen bonds and the ammonium protons, respectively. Asterisks denote spinning sidebands.

phases (III and II) of letovicite exist. The phase transition III/II occurs at 265 K. At each temperature, there are two resolved peaks (Figure 8). We assigned them on the basis of chemical shifts, and our assignment is in accordance with the former work of Fechtelkord et al.,[36] who studied letovicite at temperatures over 295 K. However, those authors presented only low-resolution spectra recorded with MAS at 5 kHz.

The smaller high-frequency peak A comes from the acidic protons of the $O^-\cdots H^+\cdots O^-$ hydrogen bonds, and the larger low-frequency peak B is from the ammonium protons. Peak

(36) Fechtelkord, M.; Engelhardt, A.; Buhl, J.-Ch.; Schwalowsky, L.; Bismayer, U. *Solid State Nucl. Magn. Reson.* **2000**, *17*, 76−68.

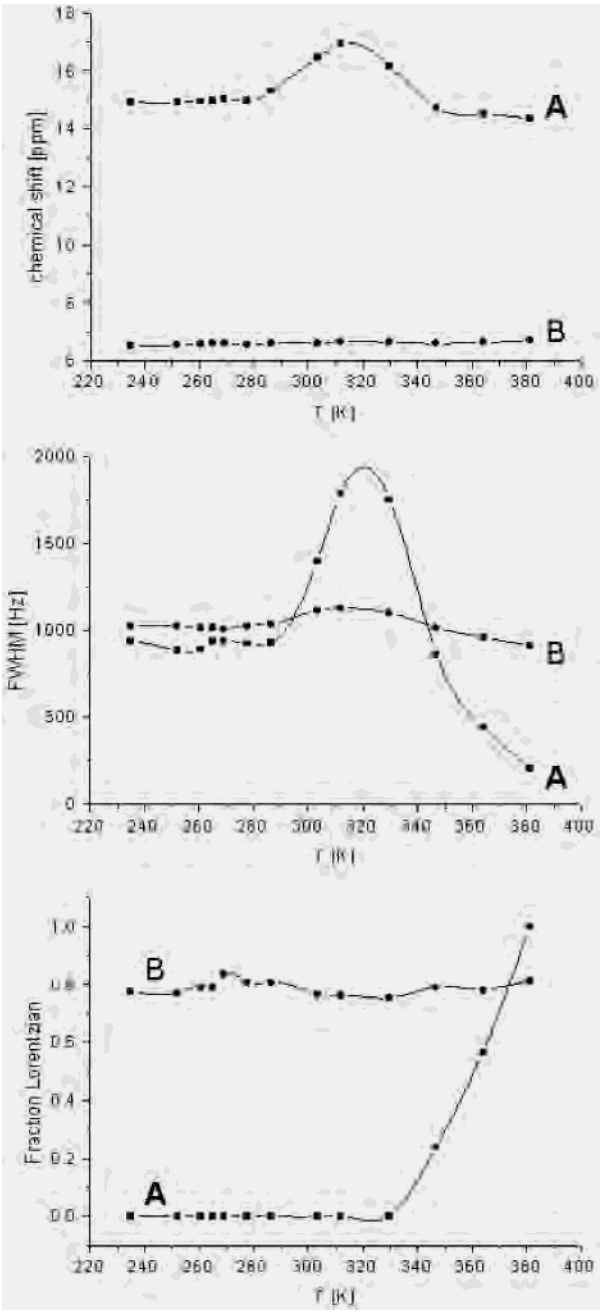

Figure 9. The temperature dependence of peak parameters for the acidic proton peak A (squares) and the ammonium peak B (circles): (a) chemical shift from TMS, (b) full width at half-maximum, (c) fraction of the Lorentzian contribution to the line shape.

A experiences great temperature effects, while peak B practically does not move or change its shape (Figure 9). It is interesting that the temperature effects on the peaks are observed beyond the phase transition temperature. Peak A appears in the 15−17 ppm range and has its maximum chemical shift at ca. 310 K (Figure 9a). Peak B appears in the chemical shift range of 6.5−6.7 ppm. The line width of peak A stays constant at ca. 900 Hz from 235 to 280 K, then increases to a maximum of ca. 1800 Hz at ca. 320 K and finally sharply decreases to 200 Hz at 381 K (Figure 9b). Peak B has its line width in the range of 900−1100 Hz with a less pronounced maximum, also at ca. 320 K. Peak A is Gaussian up to ca. 320 K and then dramatically changes its shape to Lorentzian, reaching the pure Lorentzian shape at 381 K (Figure 9c). Peak B retains a mixed shape, ca. 80% Lorentzian. Peak A has noticeable rotational sidebands only at the lowest temperatures, while the relative intensity of rotational sidebands from peak B is less affected by temperature (Figure 8).

The temperature effects observed for peak A of letovicite are indicative of the proton dynamics in the $O^-\cdots H^+\cdots O^-$ hydrogen bonds. In phase III, existing below 265 K, the proton of this hydrogen bond is located asymmetrically close to one of the sulfate oxygens (Figures 1b and 5b). The asymmetric location of the proton increases the chemical shift anisotropy, and because of that, peak A has, at low temperature, noticeable rotational sidebands (Figure 8b). The spread of chemical shifts among crystallites gives the Gaussian shape, while the chemical shift and line width remain almost constant (Figure 9). Over 265 K, the material becomes phase II. The $O^-\cdots H^+\cdots O^-$ protons start jumping between the oxygens atoms. This process becomes faster with increase of temperature. The first effect on the peak width and chemical shift is observed at ca. 280 K. The exchange between two asymmetric proton positions is initially slow, which increases the line width and the chemical shift up to ca. 320 K. At this stage, the exchange is not yet able to reduce chemical shift anisotropy. Then, the exchange becomes fast enough to considerably reduce the line width, to average out the chemical shift to more isotropic value, and to change the line shape from Gaussian to Lorenztian. Thus, the proton MAS NMR supports model II of phase II (Figure 1a).

Conclusions

In conclusion, we want to stress that triammonium hydrogen disulfate occurring in at least seven different phases is an excellent example of a structure the properties of which depend on fine details of hydrogen bonding. According to our results:

1. The proper space group for phase II is *C*2/*c*, for phases III and IV is *P*2/*n*, and for phase V is $P\bar{1}$. The structures of phases III and IV seem to be the same, according to the experimental procedure applied in this work.

2. The hydrogen atom participating in the $O^-{-}H^+\cdots O^-$ H-bond in phase II of $(NH_4^+)_3H^+(SO_4^{2-})_2$ at room temperature (rt) is split at two positions around the center of the crucial $O^-{-}H^+\cdots O^-$ H-bonding joining two SO_4^{2-} tetrahedra. With decreasing temperature, it becomes localized at only one position at one of the oxygen atoms. Then, the symmetry between the sulfate ions is broken, thus influencing the S−O distances. Further cooling causes additional differentiation of possibly equivalent sulfate dimers.

3. The NH_4^+ ions participate mainly in bifurcated H-bonds with two oxygen atoms from sulfate anions. On cooling, the major contribution of the bifurcated H-bond becomes stronger, whereas the minor one becomes weaker. This phenomenon is coupled with rotation of the sulfate ions.

4. In phase IV of $(NH_4^+)_3H^+(SO_4^{2-})_2$, but also in the other phases, additional weak but significant reflections are observed. They are located between the layers of the

reciprocal lattice suggesting possible modulation of the host $(NH_4^+)_3H^+(SO_4^{2-})_2$ structure(s).

5. Both structural parameters as well as the space group symmetry of $(NH_4^+)_3H^+(SO_4^{2-})_2$ are very sensitive to the range of diffraction angle applied during data collection.

6. According to ^1H MAS NMR obtained for phases II and III, the nature of the acidic proton disorder is dynamic and localization of the proton takes place in a broader range of temperatures as can be expected from the X-ray diffraction data.

Finally, we want to stress that in order to obtain reliable results in the case of such systems as $(NH_4^+)_3H^+(SO_4^{2-})_2$ (and similar ones), it is particularly important that not only diffractional methods but also some complementary techniques—independent of symmetry assumptions—should be applied, such as solid-state NMR spectroscopy.

Acknowledgment. The Polish State KBN Committee is thanked for a financial support to purchase a CCD diffractometer. The X-ray measurements were undertaken in the Crystallographic Unit of the Physical Chemistry Lab at the Chemistry Department of the University of Warsaw. We thank Dr. Victor A. Sarin from the Institute for Neutron Research RAS, Troitsk, Russia and Dr Lev S. Smirnov from the Institute of Theoretical and Experimental Physics, Moscow, Russia, and the I. M. Frank Laboratory of Neutron Physics JINR, Dubna, Moscow Region, Russia, for supplying excellent crystals of triammonium hydrogen disulfate $(NH_4^+)_3H^+(SO_4^{2-})_2$.

Supporting Information Available: Geometry of N−H···O$^-$ H-bonds (Table S1) and four X-ray crystallographic files in CIF format for the crystal structures of all phases studied. This material is available free of charge via the Internet at http://pubs.acs.org.

IC025705B